doi:10.1016/j.jmb.2012.06.038 J. Mol. Biol. (2012) 423, 17–33

Contents lists available at www.sciencedirect.com

Journal of Molecular Biology

journal homepage: http://ees.elsevier.com.jmb

Insights into the Regulatory Landscape of the Lysine Riboswitch

Andrew D. Garst, Ely B. Porter and Robert T. Batey*

Department of Chemistry and Biochemistry, University of Colorado at Boulder, 596 UCB, Boulder, CO 80309–0596, USA

Received 23 April 2012; received in revised form 21 June 2012; accepted 26 June 2012
Available online 3 July 2012

Edited by D. E. Draper

Keywords:
riboswitch;
transcriptional regulation;
RNA structure;
X-ray crystallography;
kinetics

A prevalent means of regulating gene expression in bacteria is by riboswitches found within mRNA leader sequences. Like protein repressors, these RNA elements must bind an effector molecule with high specificity against a background of other cellular metabolites of similar chemical structure to elicit the appropriate regulatory response. Current crystal structures of the lysine riboswitch do not provide a complete understanding of selectivity as recognition is substantially mediated through main-chain atoms of the amino acid. Using a directed set of lysine analogs and other amino acids, we have determined the relative contributions of the polar functional groups to binding affinity and the regulatory response. Our results reveal that the lysine riboswitch has >1000-fold specificity for lysine over other amino acids. The aptamer is highly sensitive to the precise placement of the ε-amino group and relatively tolerant of alterations to the main-chain functional groups in order to achieve this specificity. At low nucleotide triphosphate (NTP) concentrations, we observe good agreement between the half-maximal regulatory activity (T_{50}) and the affinity of the receptor for lysine (K_d), as well as many of its analogs. However, above 400 μM [NTP], the concentration of lysine required to elicit transcription termination rises, moving into the riboswitch into a kinetic control regime. These data demonstrate that, under physiologically relevant conditions, riboswitches can integrate both effector and NTP concentrations to generate a regulatory response appropriate for global metabolic state of the cell.

Introduction

Nonprotein coding RNA regions in mRNAs play a number of critical roles in determining its expression fate. In bacteria, one of the most pervasive types of mRNA regulatory elements discovered thus far are riboswitches, sequences found in the 5′ leader that control gene expression in response to direct binding of a small molecule.[1,2] These effectors include a diverse array of molecules such as amino acids,[1,2] purine nucleobases,[3–5] amino sugars,[6] and a variety of enzymatic cofactors and secondary messenger molecules.[7–9] Most riboswitches contain two modular domains that perform the functions of ligand binding (the aptamer domain) and regulation (the

*Corresponding author. E-mail address: robert.batey@colorado.edu.

Abbreviations used: 2AP, 2-aminopurine; 6ACA, 6-aminocaproic acid; ACL, *N*-ε-acetyl lysine; EDTA, ethylenediaminetetraacetic acid; FL, *N*-ε-formyl lysine; FMN, flavin mononucleotide; IEL, *N*-ε-iminoethyl-lysine; ITC, isothermal titration calorimetry; NMIA, *N*-methylisatoic anhydride; NML, *N*-methyl lysine; NTP, nucleotide triphosphate; PDB, Protein Data Bank; RNAP, RNA polymerase; SAM, *S*-adenosylmethionine.

0022-2836/$ - see front matter © 2012 Elsevier Ltd. All rights reserved.

expression platform). Communication between these domains is mediated by a ligand-dependent partitioning of a small sequence to either the aptamer domain or the expression platform. This partitioning determines the secondary structure adopted by the expression platform that dictates the regulatory outcome (Fig. 1a).

Considerable effort has been invested in deciphering the structural features of riboswitch aptamer domains that enable the mRNA to bind the effector with both high affinity and specificity to achieve precise genetic control against a background of highly similar chemicals in the cell. For example, purine riboswitches distinguish between guanine and adenine with >20,000-fold specificity based on the identity of a single pyrimidine that base pairs with the purine ligand.[4,5] Likewise, the various classes of *S*-adenosylmethionine (SAM) binding riboswitches discriminate SAM from *S*-adenosylhomocysteine, a toxic by-product of SAM methylation reactions, through electrostatic interactions with the sulfonium ion of SAM.[10–13] Displacement of critical carbonyls away from the sulfonium ion leads to a dramatic loss in the ability of the SAM-I riboswitch to discriminate between the two compounds.[10] Specificity can also be mediated in part by associated solvent and ions tightly coordinated with the ligand–RNA interaction, as observed in the flavin mononucleotide (FMN), thiamine pyrophosphate, and lysine riboswitches.[14–17] Due to the fact that many riboswitches control the production or uptake of metabolites critical for normal growth and reproduction, these RNAs are considered to be potentially important therapeutic targets for disrupting microbial metabolism.[18] Knowledge on the mechanisms by which effector specificity is achieved by riboswitches informs our understanding on patterns of gene regulation in bacteria and is essential for guiding rational design of novel compounds to target these RNAs as potential antimicrobials.

An additional constraint encountered by many riboswitches is that they must function within a short time frame. This limitation arises in transcription attenuation where a regulatory decision must be made when the RNA polymerase (RNAP) reaches the intrinsic transcriptional terminator.[19] Thus, the rates of ligand association and dissociation can significantly influence the concentration of effector required to elicit a regulatory response. This kinetic constraint is thought to account for the observation that many riboswitches require ligand

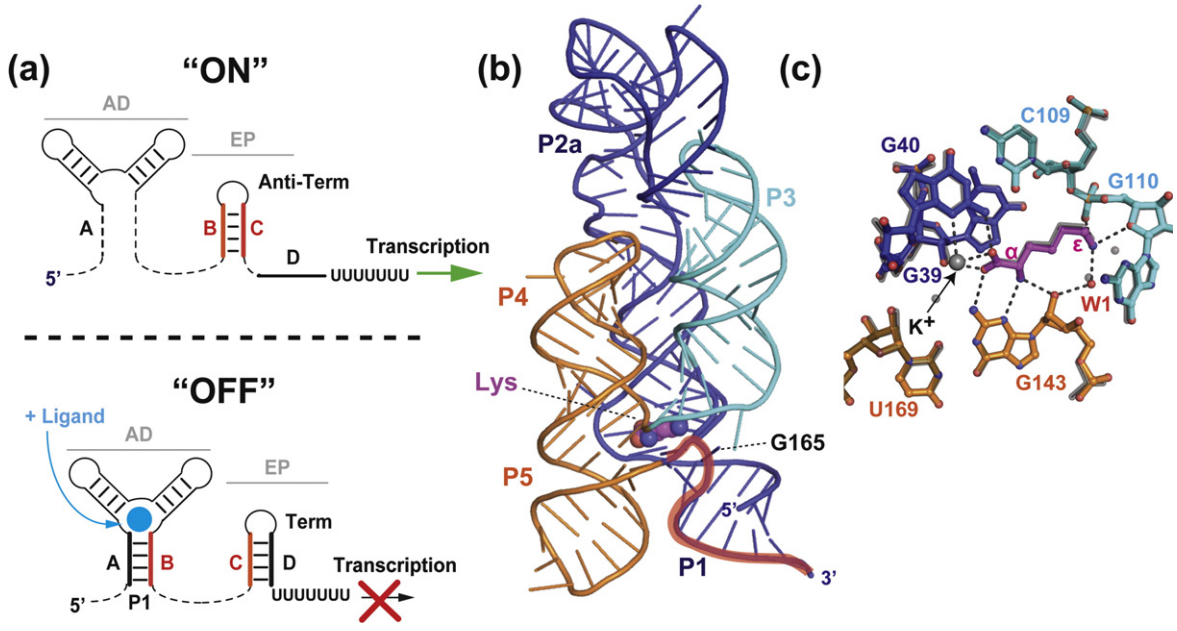

Fig. 1. (a) Schematic of riboswitch-mediated transcriptional regulation emphasizing the nature of the mutually exclusive secondary structural switch. (b) Global tertiary structure of the lysine riboswitch observed by X-ray crystallography (PDB ID: 3D0U). The three sets of coaxially stacked helices are shown in different colors, and lysine is shown in magenta in the five-way junction. The switching sequence at the 3′ side of P1 is highlighted in red. (c) Lysine binding site within the central junction showing an overlay of the binding pockets of two independently solved crystal structures[17,38] (PDB ID: 3D0U, colored; PDB ID: 3DIL, gray). The ε-amino group of lysine forms electrostatic contacts with the backbone of G110 and an ordered solvent molecule (W1) that was observed in both of the original crystallographic studies of this RNA. The main-chain atoms hydrogen bond with G143 and coordinate to a potassium ion near G40. A cavity exists beyond the carboxyl terminus that is occupied by ordered solvent when bound to lysine.

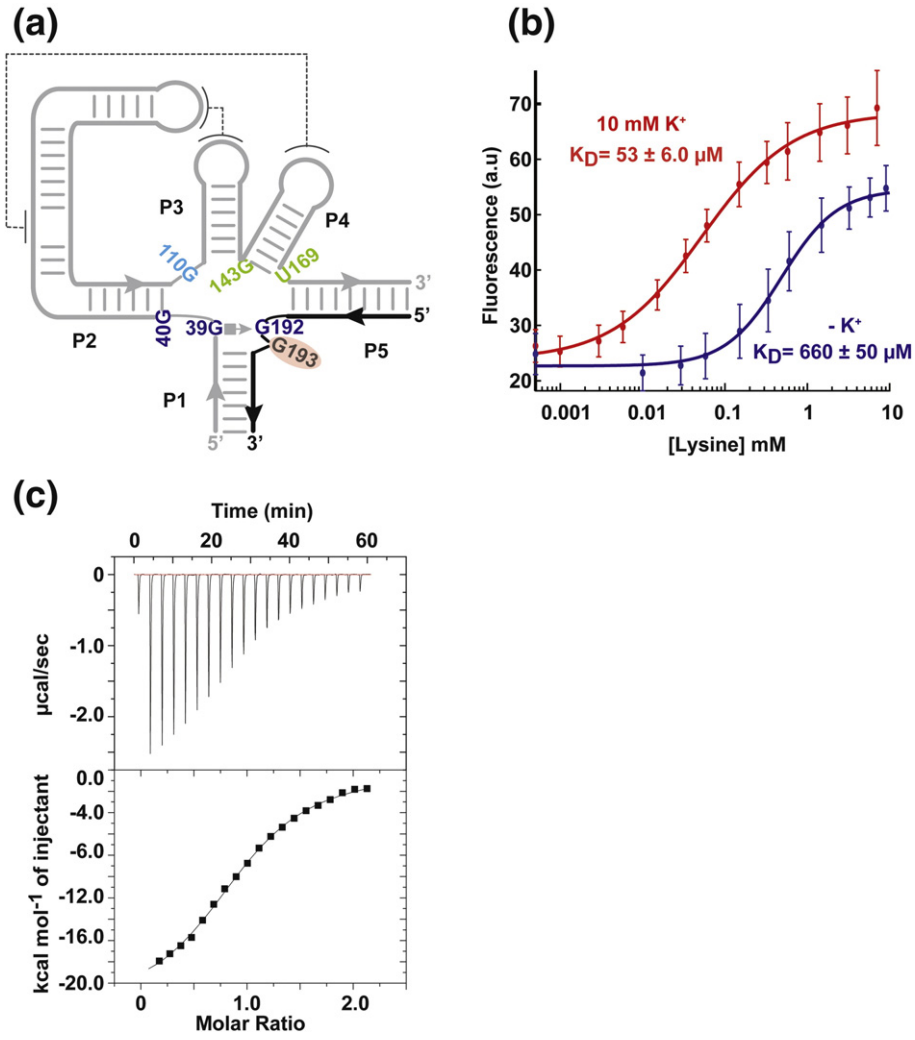

Fig. 2. (a) Cartoon of the two-piece 2AP reporter construct used for the binding studies presented in this paper. The gray and black strands were annealed as described in Materials and Methods to reconstitute a functional RNA for fluorescence-based assays. The site of 2AP fluorophore substitution is at G193. Colored nucleotide positions correspond to the lysine binding pocket in Fig. 1c. (b) Fluorescence data from lysine titrations with the 2AP-labeled construct in the presence (red) or in the absence (blue) of 10 mM KCl. Note the decrease in both binding affinity and change in fluorescence upon omission of KCl from the buffer. (c) Lysine binding to the wild-type *lysC* aptamer as measured by ITC demonstrates reasonable agreement between the K_d values for the 2AP-labeled construct and the native RNA.

concentrations much greater than the equilibrium binding constant (K_d) to effectively regulate transcription, a phenomenon termed "kinetic control".[20] This is in contrast with "thermodynamic control" in which the concentration of the effector to half-saturate the aptamer is equal to the concentration of effector required to elicit a half-maximal regulatory response (T_{50}). For example, a detailed analysis of the FMN riboswitch demonstrated that the T_{50} for this RNA is ~10- to 100-fold in excess of the K_d,[21] which was attributed to the slow binding kinetics of FMN. Similar observations have been made for the guanine,[22] lysine,[23–25] SAM-I,[26] cyclic diguanylate,[27] and tetrahydrofolate[28] riboswitches, suggesting that kinetic control may be a general feature of all riboswitches that act through transcriptional attenuation.

While it is tempting to make this generalization, many factors influence the rate of transcription and thus the regulatory time frame. For example, intrinsic pause sites,[29] transcription factors such as NusA and NusG,[30,31] and nucleotide triphosphate (NTP) concentrations have all been demonstrated to influence pausing and transcriptional attenuation.[21,32] The degree to which these factors can exert their regulatory influence, however, remains poorly understood. For example, the intracellular concentration of NTPs varies by factor of 2- to 5-fold during different bacterial growth phases,[33] playing a central role in regulating the transcription

of pyrimidine biosynthetic genes,[34] ribosomal RNA,[35] and a variety of other processes.[34,36,37] Most studies of transcriptional regulation by riboswitches, however, have focused on limited conditions thereby ignoring a potentially important aspects of the regulatory landscape.

To explore the relationship between equilibrium affinity (K_d), binding kinetics (k_{on} and k_{off}), and regulatory activity (T_{50}), we have examined the mechanistic details of the *Bacillus subtilis lysC* lysine-responsive riboswitch. The aptamer of this riboswitch folds into a complex structure involving the packing of multiple helices together that organize a binding pocket for lysine within a five-way junction (Fig. 1b and c).[17,38] To better define how this RNA achieves lysine specificity against a background of abundant amino acids that bear similar main-chain functionality, we have measured the K_d and binding kinetics for lysine and a number of related analogs. These data provide a benchmark for comparative analysis of the binding affinity and kinetics of the aptamer to transcriptional regulation, allowing us to examine the relationships between these parameters. Previous studies of the *B. subtilis lysC* riboswitch suggest that the T_{50} for lysine is ~1000-fold greater than K_d.[23,24,39] However, we demonstrate that lysine promotes efficient transcriptional termination with a T_{50} equivalent to the K_d under low NTP concentrations—the hallmark of thermodynamic control. A number of lysine analogs also regulate transcriptional termination at concentrations near K_d, consistent with a simplified kinetic model of transcriptional regulation based on the observed binding rate constants. However, at >400 μM NTP concentrations, transcriptional termination requires ~5-fold higher concentrations of lysine. This suggests that the regulatory efficiency of this RNA could be tuned by the metabolic state of the cell, such as under nutrient limiting conditions. Under high [NTP], the riboswitch also exhibits a greater degree of selectivity for lysine over non-cognate ligands with the exception of two of the main-chain derivatives whose rapid binding kinetics appear to render them insensitive to transcription speeds.

Results

Characterization and validation of a 2-aminopurine-labeled receptor

To establish the apparent equilibrium dissociation constant ($K_{d,app}$) for each of the compounds used in this study, we site specifically labeled a two-piece aptamer derived from the *B. subtilis lysC* riboswitch.

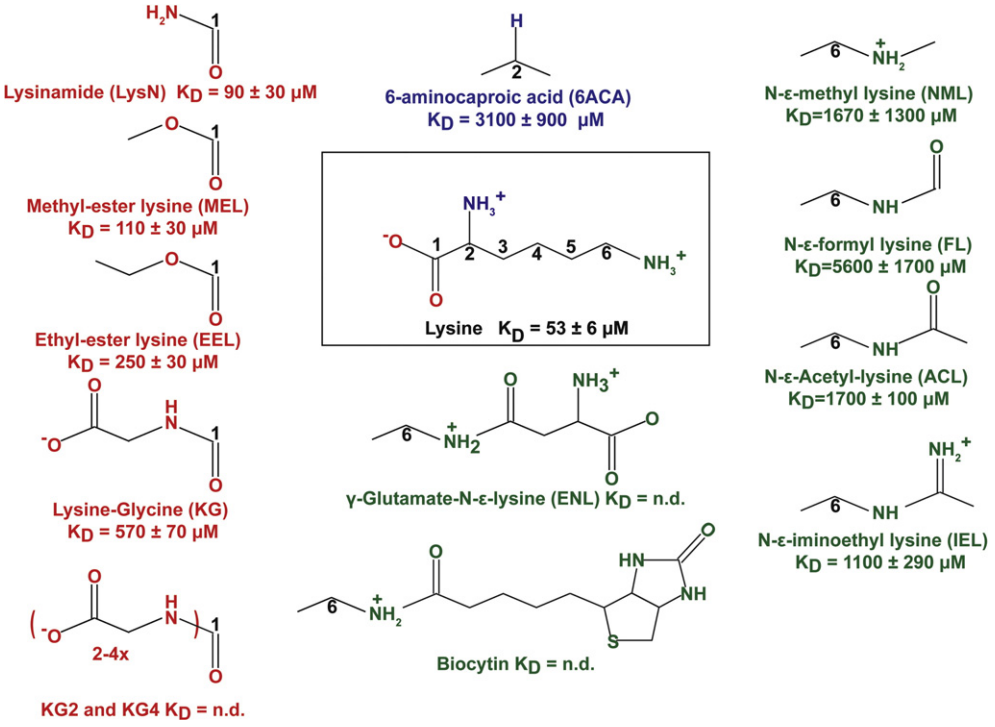

Fig. 3. Structures of select compounds used in this study. The functional group changes relative to lysine are depicted for each compound and colored corresponding to the carboxylate (red), main-chain amine (blue), and ε-amine (green), respectively. The abbreviation for each compound used in the text is given in parentheses. The observed equilibrium dissociation constant (K_d) as measured by the 2AP fluorescence assay is given for each compound.

Table 1. Affinity and free-energy measurements of ligand binding to the *B. subtilis lysC* aptamer

Ligand	K_d (μM)	K_{rel}[a]	$\Delta\Delta G°$ (kcal/mol)
Lysine	53 ± 6	1.0	0.0
Lys(−KCl)	480 ± 40	9.1	1.4
LysN	90 ± 30	1.7	0.3
MEL	110 ± 30	2.1	0.4
EEL	250 ± 30	4.7	1.0
KG	570 ± 70	11	1.5
6ACA	3100 ± 900	58	2.5
NML	1670 ± 300	32	2.1
IEL	1100 ± 290	21	1.9
ACL	1700 ± 100	32	2.1
FL	5600 ± 1700	106	2.9

[a] $K_{rel} = K_{d,analog}/K_{d,lysine}$.

A fluorescent 2-aminopurine (2AP) nucleotide was incorporated at a non-conserved position in the five-way junction (G193; Fig. 2a). Chemical footprinting studies have demonstrated that this position undergoes a significant conformational change upon lysine binding[25,38] and is solvent exposed in the crystal structure.[17,38] These data imply that this nucleotide transitions from a stacked conformation with other nucleotides in the unbound aptamer to a solvent-exposed conformation upon lysine binding. This is further supported by a previous study from Blouin and Lafontaine that also used a 2AP reporter at this position to monitor the effects of Mg^{2+} on global folding of the RNA.[23] As expected, a strong increase in fluorescence was observed upon the addition of lysine consistent with the labeled position becoming flipped out into solution upon binding (Fig. 2b). Fitting the data to a simple two-state binding model yielded a $K_{d,app}$ for lysine of 53 ± 6 μM at 37 °C (Table 1).

The affinity of lysine for the 2AP reporter is significantly weaker than previous reports.[17,25,39] However, folding and ligand binding by the lysine aptamer have been shown to exhibit a strong Mg^{2+} dependence,[17,23,40] suggesting that our choice of experimental conditions could be responsible for this discrepancy. To differentiate between this and the possibility that our two-piece construct design perturbs ligand binding, we measured the affinity of lysine for the wild-type *B. subtilis lysC* aptamer domain (nucleotides 32–199; Fig. S1) under the same experimental conditions using isothermal titration calorimetry (ITC). A $K_{d,app}$ of 18 ± 2.2 μM was measured for lysine at 37 °C (Fig. 2c), within ~3-fold of the 2AP reporter. The measured $\Delta H° = -21 \pm 1.6$ kcal/mol and $-T\Delta S° = 15 \pm 2.0$ kcal/mol are comparable to values obtained of other riboswitch aptamer–ligand interactions[4,10,41] and agree well with previous ITC data of the lysine riboswitch derived from *Clostridium acetobutylicum*,[41] reflecting a highly enthalpically driven binding event.

As a second test of the validity of the 2AP reporter, the effect of potassium on lysine binding was measured. This ion mediates recognition of the α-carboxy group of lysine (Fig. 1c) and was shown to enhance lysine binding affinity in previous biochemical studies.[17] Substitution of potassium with sodium under our buffer conditions results in an ~10-fold decrease in affinity (Fig. 2b), confirming the importance of this monovalent cation in mediating a high-affinity interaction. Interestingly, comparison of absolute fluorescence between the two monovalent cations suggests that K^+ selectively stabilizes the flipped out conformation of the 2AP reporter as evidenced by the increased change in fluorescence at saturating lysine, while having no apparent effect on the unliganded state. This interpretation is consistent with primer extension assays demonstrating

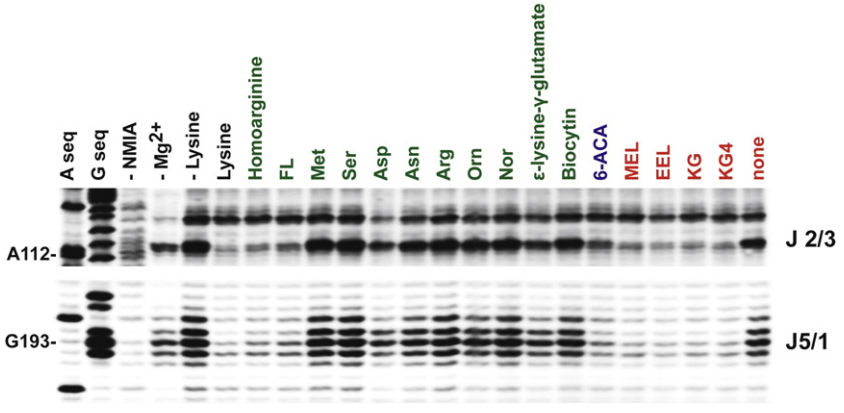

Fig. 4. Chemical probing of the lysine riboswitch using NMIA in the presence of either 1 mM lysine or 10 mM subset of the analogs from this study. In the absence of ligand (the −lysine lane), the high reactivity of the J2/3 and J5/1 regions indicate local flexibility of the RNA backbone. Addition of lysine or a binding-competent ligand protects these regions from NMIA modification. Labels colored according to the R1, R2, and R3 schemes in Fig. 3. Nucleotides A112 and G193 are labeled for reference according to the numbering scheme in Fig. S1.Chemical probing of the lysine riboswitch using NMIA in the presence of either 1 mM lysine or 10 mM subset of the analogs from this study. In the absence of ligand (the −lysine lane), the high reactivity of the J2/3 and J5/1 regions indicate local flexibility of the RNA backbone. Addition of lysine or a binding-competent ligand protects these regions from NMIA modification. Labels colored according to the R1, R2, and R3 schemes in Fig. 3. Nucleotides A112 and G193 are labeled for reference according to the numbering scheme in Fig. S1.

that potassium has no effect on reverse transcriptase pausing in the absence of lysine[17] and suggests that this ion is recruited specifically to the RNA–ligand complex as opposed to stabilizing preformed structures in the unliganded aptamer.

Molecular determinants of specificity

In their cellular context, riboswitches must contend with a complex chemical environment that challenges their ability to coordinate gene expression in response to a specific effector. Recent studies have provided evidence that some riboswitch aptamers can bind alternative cellular ligands. For example, binding different hexose sugars has been demonstrated to inhibit glucose-6-phosphate-dependent cleavage by the *glmS* riboswitch *in vitro* and *in vivo*,[42] thereby enabling the riboswitch to integrate multiple cellular cues into a single regulatory output. While selectivity of the lysine riboswitch appears to be determined by an electrostatic interaction with the ε-amino group of lysine (Fig. 1c), the α-amine and carboxylate groups provide a significant recognition surface that might support binding of alternative amino acids. Docking of the other standard amino acids into the binding pocket, which is assumed to be rigid, suggests that the side chain of many of these molecules could also potentially form favorable interactions with the RNA (Fig. S2a).

To determine whether the lysine aptamer can productively bind other amino acids, we tested a subset of the proteogenic amino acids that have high intracellular concentrations[43] and are complementary to the RNA binding site (Fig. S2a). Most of these amino acids, including alanine, asparagine, threonine, and methionine, showed no fluorescence change in the 2AP-labeled aptamer (Fig. S2b). Only serine displayed some binding, albeit with extremely low affinity (>20 mM), well above its intracellular concentration (~70 μM[43]). This is consistent with the observation that nonstandard amino acids such as ornithine or norleucine that displace or remove the ε-amine are also unable to bind this RNA.[25] Thus, the backbone atoms, while certainly contributing to binding affinity of lysine, are insufficient on their own. Furthermore, these data argue that positioning of the amino group adjacent to the G110 phosphate and O4′-ribosyl oxygen (Fig. 1c) is the primary basis for discrimination against the abundant amino acids present in the cell.

To specifically address the thermodynamic contributions of each polar functional group, we next measured the binding affinity of a set of compounds that systematically test key features of the binding interface (Fig. 3 and Table 1). From previous crystallographic studies, there are two sets of interactions between the ε-amino group and the RNA hypothesized to be important: an electrostatic interaction between the amine and the non-bridging phosphate oxygen of G110 and a water-mediated interaction between the amine and the 2′-OH of G143. Since the 2′-OH of G143 also interacts with the α-amino group of lysine, the hydroxyl group acts as a hydrogen bond donor to this water (W1; Fig. 1c). The importance of the water was assessed using *N*-methyl lysine (NML), which maintains the position and charge of the side-chain amine, but is expected to displace W1 in order to accommodate the additional methyl group within the binding site. The ~34-fold decrease in affinity of NML relative to lysine verifies that this water accounts for a significant energetic contact with the side chain.

To further address the contribution of the side chain to binding energetics, we tested a set of compounds that perturb the presence and localization of the positive charge without displacing the amine (Fig. 3): *N*-ε-formyl lysine (FL), *N*-ε-acetyl lysine (ACL), and *N*-ε-iminoethyl-lysine (IEL). FL and ACL ablate the positive charge on the nitrogen, as well as adding steric bulk to the ε-amino group. Structures of homoarginine and IEL bound to this RNA[17] suggest that the additional functionality of FL and ACL would displace a water molecule (W1) with a carbonyl oxygen that could act as a hydrogen bond acceptor from the 2′-OH group of G143 (Fig. 1c). Surprisingly, despite lacking a formal charge on the side chain, these compounds exhibit only a 4.5-fold loss in affinity relative to NML. This clearly shows that the positive charge of the amino group is not essential for productive binding, particularly if extended hydrogen bonding contacts are maintained. Most of the energetic penalty associated with these compounds can presumably be accounted for by their additional steric bulk, as evidenced by IEL that can localize positive charge to the ε-amino group but binds only ~2-fold better than NML and ~10-fold worse than lysine. Together, these data argue that both positive charge and water-mediated interactions cooperate to provide optimal ligand recognition. We also found that the addition of very large functional groups to the ε-amino group of lysine, such as those found in biocytin and γ-glutamate-ε-*N*-lysine, is not tolerated (Fig. 3), indicating that the binding pocket cannot rearrange to accommodate bulkier modifications to the side chain.

In contrast to the side chain, the main-chain functional groups of lysine appear to play a lesser role in establishing a high-affinity interaction with the lysine riboswitch aptamer domain. For example, compared with a >5 kcal/mol penalty associated with deletion of the ε-amine, deletion of the α-amine [6-aminocaproic acid (6ACA); Fig. 3] carries an energetic penalty of only 2.5 kcal/mol corresponding to loss of hydrogen bonding with the N3 and 2′-OH groups of G143 (Fig. 1c). Furthermore, the α-carboxyl group appears to be particularly tolerant to

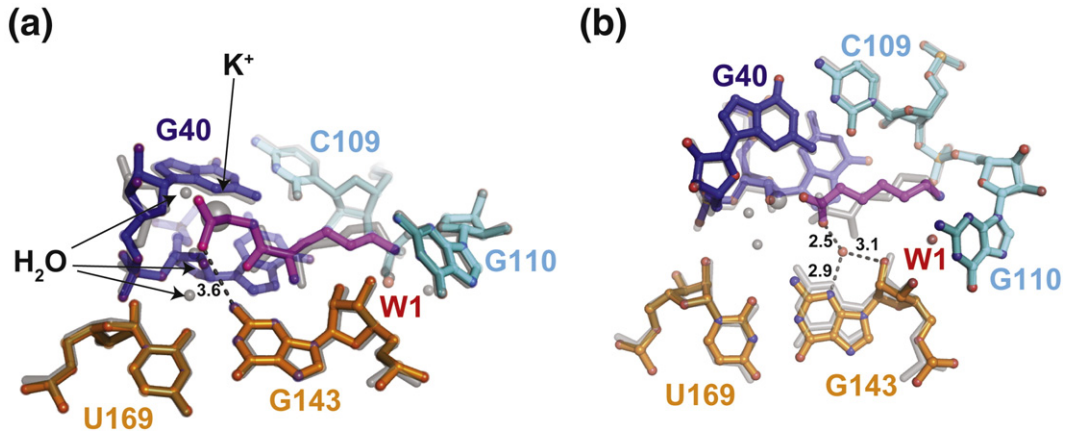

Fig. 5. Structures of (a) KG and (b) 6ACA bound to the lysine binding pocket in the *T. maritima* lysine riboswitch. The structure of the RNA–lysine complex (PDB ID: 3DIL) is superimposed in each panel (colored gray) for reference. In each of the two structures, the RNA adopts an identical conformation on both global and local levels, consistent with chemical probing. (a) The glycyl residue in KG displaces solvent- and ion-occupied positions (gray spheres) identified in the lysine-bound structure but does not appear to clash significantly with the RNA. (b) Removal of the main-chain amine of lysine in 6ACA results in the recruitment of a water to replace the hydrogen bonding interactions that are lost between the ligand and the N3 and 2′-OH groups of nucleotide G114. The carboxylate group of 6ACA shifts over slightly to coordinate this water. Unique hydrogen bonding interactions for each ligand are shown by gray broken lines labeled with distances in angstroms.

modification as exemplified by the small energetic penalties (≤1.5 kcal/mol) associated with the alteration of this functional group. For example, neutralization of the carboxylate with the analog lysinamide (LysN) causes no loss in binding affinity, despite the likelihood that it displaces the K^+ ion adjacent to G40 (Fig. 1c). Likewise, a methyl ester (MEL) at this position decreases binding affinity by only ~3-fold. The addition of ethyl (EEL, L-lysine ethyl ester) or glycyl (KG, lysyl glycine) moieties of increased steric bulk further diminishes affinity, but not nearly to the same extent as modifications to the amino groups. Beyond a single glycine (KG dipeptide), the RNA cannot accommodate larger peptides (KG_2–KG_4), again suggesting that the flexibility of this binding site is limited.

Rigidity of the lysine binding pocket

To determine the nature of the global and local structural rearrangements of the RNA induced by the various ligands tested above, we employed a chemical probing technique known as selective 2′-hydroxyl acylation analyzed by primer extension or "SHAPE".[44] This method generally assesses local flexibility of the backbone with single nucleotide resolution based on reactivity of ribose 2′-hydroxyl groups with *N*-methylisatoic anhydride (NMIA).[45] Reactivity of NMIA is determined by the conformation of the ribose sugar bearing the 2′-hydroxyl group with the C2-endo configuration being the reactive state and has been demonstrated to strongly correlate with the NMR order parameter.[46] Nucleotides in the five-way junction exhibit high reactivity toward NMIA in the absence of ligand, indicating that this region of the RNA is conformationally flexible (Fig. 4). Addition of saturating ligand concentrations (1 mM lysine or 10 mM lysine analogs) demonstrates a similar set of chemical reactivity protections for each of the junction segments in complex with the various analogs (Fig. 4). The reactivity pattern for the majority of nucleotides is unperturbed by ligand binding (Fig. S3), consistent with the RNA adopting a preformed tertiary architecture as observed by small-angle X-ray scattering.[38,41] These data strongly argue that all of the ligands that productively bind the RNA induce the same structural rearrangements of the binding pocket.

To further investigate how main-chain derivatives are accommodated within the binding site, we determined the crystal structure of the 6ACA and KG compounds in complex with the *Thermatoga maritima* aptamer using X-ray crystallography. With the exception of G193, a nucleotide that is flipped out toward solution and phylogenetically variable, the sequence of the ligand-binding core of the *T. maritima* and *B. subtilis* lysine aptamers are identical (Fig. S4).Thus, interpretation of structures of the *T. maritima* aptamer bound to various ligands is highly likely to be valid for the *B. subtilis* riboswitch. These crystals diffracted to ~3.0 Å resolution, and models were generated by standard molecular placement methods using the free-state lysine riboswitch structure in which solvent molecules and nucleotides around the binding pocket

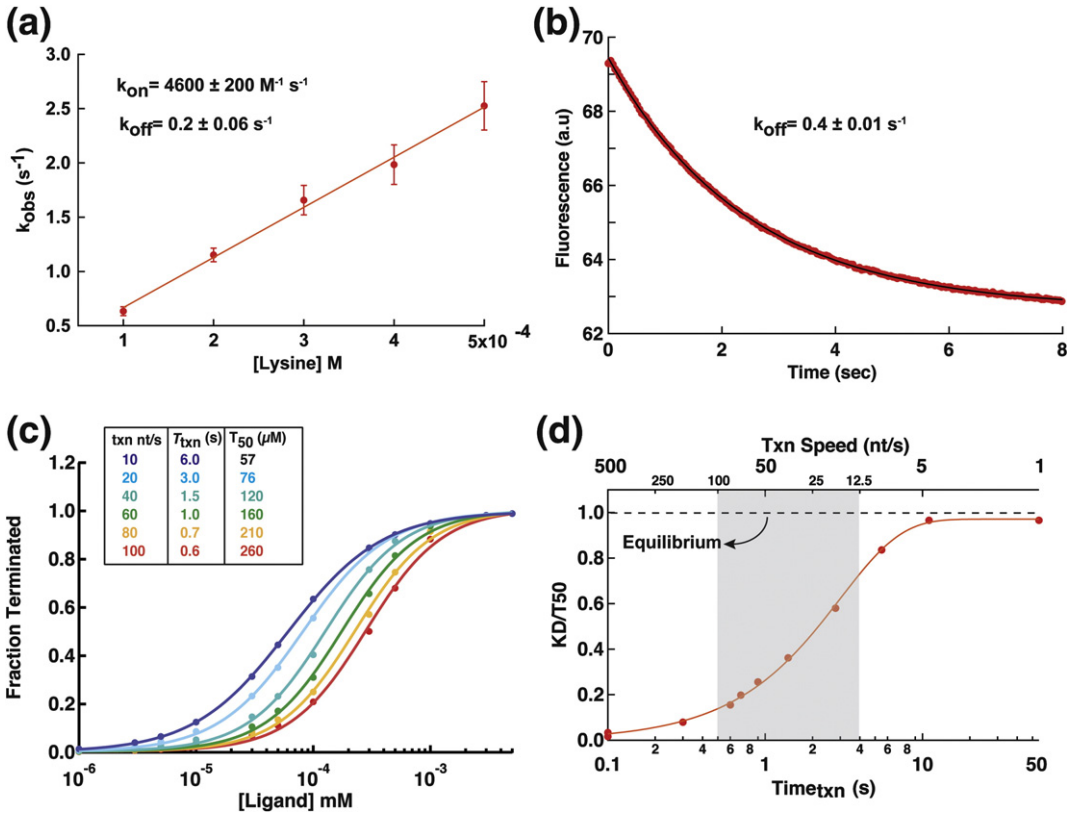

Fig. 6. Analysis of lysine binding kinetics by stopped-flow fluorescence spectroscopy. (a) Fit to the observed binding rate (k_{obs}) as a function of lysine concentration. The slope of the fit yields the association rate constant (k_{on}), while the y-intercept of this line yields an estimate of the k_{off}. (b) Direct measurement of k_{off} measured by rapid dilution of pre-incubated RNA–ligand complexes into buffer. The data shown represent an average of five injections. (c) Calculation of the fraction of riboswitch bound by lysine at different equilibration times using the experimentally observed k_{on} and k_{off}. At a long equilibration time, corresponding to a slow rate of transcription (dark blue), the fit to the curve yields a T_{50} that is equal to K_d. As the time allowed for the aptamer to equilibrate with ligand decreases, the calculated T_{50} increases (from light blue to red), indicating kinetic control. (d) Plot of the K_d/T_{50} ratio as a function of rate of transcription or equilibration time shows that the reaction becomes fully equilibrated by 10 s (as the ratio approaches 1), with appreciable approach to equilibration after 3–5 s. The K_d/T_{50} ratio is expected to vary by 4- to 5-fold over a range of physiologically relevant transcription speeds as denoted by the gray box.

were removed [Protein Data Bank (PDB) ID: 3D0X] (crystallographic and model statistics are detailed in Supplementary Table 1). Maximum-likelihood superimposition of the refined models (Fig. 5) with the original lysine-bound RNA using THESEUS[47] revealed that the RNA adopts an identical fold when bound to these analogs as inferred from the chemical probing analysis (Fig. 4). The average displacement of all of the atoms within the binding pocket was less than the coordinate error of the structure.

The structures of the main-chain derivatives reveal that these compounds orient themselves within the rigid pocket to maximize hydrogen bonding interactions with the RNA. In the KG–RNA complex, the glycine residue of the dipeptide is clearly identifiable in simulated annealing omit maps (Fig. S5), extending an additional 3.6 Å away from the central cavity of the RNA. The terminal carboxyl group of the dipeptide appears to form a hydrogen bond with the 2′-hydroxyl group of G143 at the base of the P4 helix (Fig. 5a). Interestingly, the interaction replaces an ordered solvent molecule that coordinates to the K^+ ion when lysine is bound, indicating that water-mediated contacts may be important in multiple facets of the binding interface. In the 6ACA-bound structure, the simulated annealing omit maps reveal two distinct peaks of density in the binding pocket (Fig. S5). One peak can be clearly distinguished as the 6ACA compound while the second peak was modeled as water (Fig. 5b and Fig. S5). The carboxyl group of 6ACA is positioned adjacent to a well-ordered solvent molecule and within hydrogen bonding distance to the sugar edge of G143 at the base of P4, thereby replacing

interactions lost by removal of the α-amino group of lysine. The overall similarity of the junction bound to these analogs suggests that this element is relatively rigid and requires that lysine analogs adapt to the binding site by either formation of new hydrogen bonding interactions or recruiting ordered solvent to mediate ligand–RNA contacts. This is consistent with previous results from Serganov *et al.* in which the various side-chain analogs stabilized an identical RNA conformation.[17]

Binding kinetics suggest a rapid approach to equilibrium

The activity of riboswitches that regulate transcription has been shown to be influenced by the kinetic properties of ligand binding such that the concentration of effector required to elicit the half-maximal regulatory response (T_{50}) can be significantly higher than the concentration needed to half-saturate the aptamer domain (K_d).[48] To define the relationship between binding and activity of the *B. subtilis lysC* riboswitch, we measured the kinetic parameters of lysine binding using stopped-flow experiments that monitor changes in fluorescence of the 2AP-labeled lysine aptamer as a function of time. Lysine association and dissociation was measured under identical conditions as K_d measurements [50 mM Tris–HCl (pH 8.0), 100 mM NaCl, 10 mM KCl, 5 mM $MgCl_2$, and 0.1 mM ethylenediaminetetraacetic acid (EDTA) at 37 °C] using pseudo-first-order conditions under which the ligand is in excess over the labeled RNA.[49] The observed rate of association (k_{obs}) was measured under a variety of lysine concentrations, and the data fit to a linear equation to obtain estimates of $k_{on} = 4600 \pm 200\ M^{-1}\ s^{-1}$ and $k_{off} = 0.2 \pm 0.06\ s^{-1}$ for this RNA (Fig. 6a). Direct measurement of k_{off} using a rapid dilution approach in which the preformed complex is diluted with an equal volume of buffer yields a comparable value of $0.4 \pm 0.01\ s^{-1}$ (Fig. 6b).

Kinetic measurements for a representative set of lysine analogs reveal that most modifications to the ligand slow the association kinetics (k_{on}) by at least an order of magnitude (Table 2). The most significant drop in the association rate is observed with ACL that abrogates the electrostatic interaction between the side chain and RNA. Conversely, LysN exhibits an ~40-fold increase in the association rate over lysine. One explanation for this observed trend is that it correlates to the net charge of the ligand, with each increase in the net charge by +1, resulting in substantial increase in k_{on}. Direct dissociation rate (k_{off}) measurements were also made for each compound; these values are more consistent with that of lysine, except for LysN that dissociates ~200-fold more rapidly than lysine. Importantly, the K_d calculated using the observed k_{on} and k_{off} values is within ~1- to 2-fold of that obtained from equilibrium studies (Table 2). Slightly greater deviation was observed for the ACL and EEL compounds, perhaps reflecting a more complex binding mechanism not readily apparent from the current analysis.

Assuming a simple two-state model for the aptamer binding reaction, the observed binding

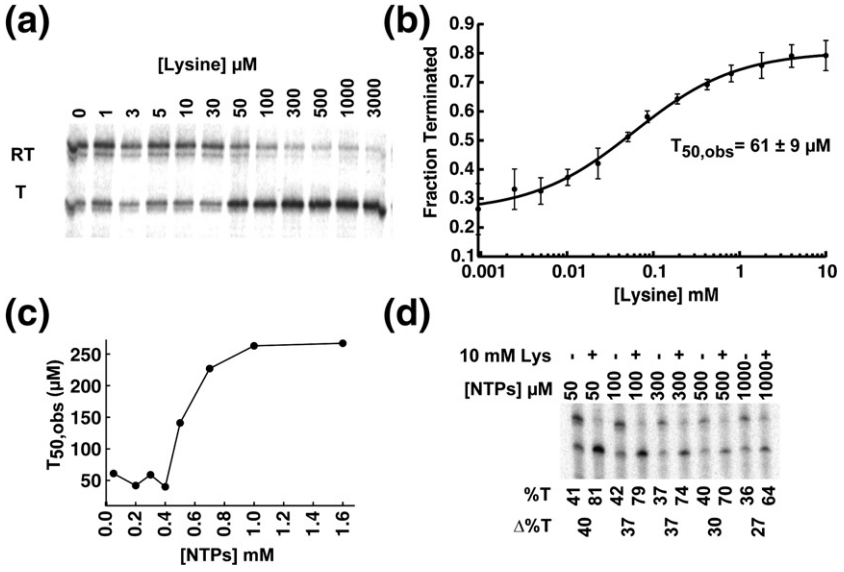

Fig. 7. Effects of transcription speed and ligand binding kinetics on transcriptional regulation. (a) Single turnover transcription of the *B. subtilis lysC* riboswitch as a function of lysine concentration. The full-length transcription product, or readthrough (RT), and the terminated (T) products were separated by denaturing gel electrophoresis and quantified as described in Materials and Methods to obtain measurements of the T_{50}. (b) Data fitting for lysine titrations performed at 50 μM NTPs. The T_{50} under these conditions closely approximates the observed K_d, indicating that binding is approximately under thermodynamic equilibrium in these conditions. (c) Influence of increasing NTP concentrations on the T_{50} for lysine. The values on the *x*-axis represent the concentration of each individual NTP. The 5-fold increase in the T_{50} is consistent with the modeling shown in Fig. 6c. (d) The efficiency of the ligand-dependent termination response decreases with increasing NTP concentrations. Combined with the increased T_{50} effect shown in (b), these data demonstrate that transcription speed modulates ligand-dependent regulation.

Table 2. Kinetics measurements of ligand binding to the *B. subtilis lysC* aptamer

Ligand	k_{off} (s^{-1})	k_{on} (M^{-1} s^{-1})	$K_{d,calc}$ (μM)	$K_{d,obs}$ (μM)	$K_{d,calc}/K_{d,obs}$	$T_{50\text{-calc}}$ (μM) (10 nt/s)	$T_{50\text{-calc}}$ (μM) (100 nt/s)
Lysine	0.25 ± 0.06	4600 ± 200	55	53 ± 6.0	1.0	57	260
EEL	0.31 ± 0.03	480 ± 15	650	250 ± 30	2.5	680	2800
KG	0.34 ± 0.03	480 ± 24	700	570 ± 70	1.6	920	2400
NML	1.1 ± 0.1	690 ± 10	1600	1670 ± 300	1.3	2200	2900
LysN	48 ± 10	186,000 ± 39,000	260	90 ± 30	3.0	260	260
ACL	0.26 ± 0.03	49 ± 5	5300	1700 ± 100	2.9	5700	26,000

rate constants (k_{obs}) can be directly related to an expected T_{50} response by the relationship:

$$T_{50-calc} = \frac{[RL]}{[R]_T}(\Delta t_{RNAP}) = \left(\frac{[L]^n}{[L]^n + K_d}\right)\left(1 - e^{k_{obs} \cdot \Delta t_{RNAP}}\right) \quad (1)$$

where $([RL]/[R]_T)(\Delta t_{RNAP})$ is the fractional saturation of the aptamer at time Δt_{RNAP} and [L] is the ligand concentration.[50] Δt_{RNAP} is defined as the time required for transcription to proceed from the 3′ end of the aptamer domain (the earliest possible time at which binding can occur, or $t = 0$) to the uridine-rich tract of the rho-independent terminator stem at the 3′ boundary of the expression platform. The 12- to 14-nt footprint of the transcription elongation complex[51] suggests that the aptamer becomes binding competent after the first 212 nt of transcription (Fig. S1). This provides an additional ~60 nt of transcript before the transcription elongation complex reaches the downstream termination site. Using physiologically realistic rates of 10–100 nt/s[52,53] for bacterial RNAP, we can therefore model theoretical T_{50} values based on this sequence length and the kinetics of ligand binding as shown previously,[50] where each individual curve represents a specific rate of transcription (Fig. 6c). The ratio of the calculated T_{50} and the measured equilibrium dissociation constant for ligand binding to the aptamer ($T_{50,calc}/K_{d,obs}$) plotted against the rate of transcription (or alternatively, Δt_{RNAP}) describes the conditions under which the riboswitch is kinetically *versus* thermodynamically controlled, where the latter is defined as $T_{50,calc}/K_{d,obs} \cong 1$ (Fig. 6d).

This analysis predicts that the *B. subtilis lysC* lysine riboswitch is under thermodynamic control when Δt_{RNAP} is ≥3–5 s, corresponding to transcription speeds of ~12–20 nt/s. This rate of transcription is in the range of that of *Escherichia coli* RNAP in the presence of NusA, a highly abundant cellular transcription factor that slows the translocation step of elongation.[54,55] On the other hand, if we assume maximal transcription rates of ~100 nt/s, these calculations predict that the T_{50} will increase by a factor of ~5-fold (from ~50 to ~260 μM). Extension of this analysis to the lysine analogs reveals that, despite large differences in k_{on}, the relatively fast dissociation kinetics of these compounds still allow a rapid approach to equilibrium relative to standard rates of transcription (Table 2). Most of the analogs also would be sensitive to Δt_{RNAP} similar to lysine, although LysN is predicted to equilibrate rapidly enough to regulate at similar concentrations regardless of transcription speed.

Analysis of transcriptional regulation and the effects of transcription speed

To test the predictions made by the above kinetic model, we used a single turnover *in vitro* transcription assay to directly measure the amounts of readthrough and terminated transcript as a function of ligand. Transcriptions were performed with *E. coli* RNAP at 50 μM NTP concentrations using a DNA template containing the genomic *B. subtilis lysC* leader sequence fused to a T7A1 promoter as described previously[56,57] (Fig. 7a). While the *E. coli* polymerase has been demonstrated to exhibit more pronounced pausing behavior than the *B. subtilis* RNAP,[36,58] previous studies of riboswitch regulation suggest that the observed T_{50} is not significantly perturbed by the choice of enzyme.[21,36,39,59]

Notably, most protocols for *in vitro* transcription assays exclude potassium from the transcription buffer and use high concentrations of Mg^{2+} (20 mM).[56,57] The lysine riboswitch is highly sensitive to both the identity and the concentration of monovalent and divalent cations,[17] which significantly influence the affinity of the *lysC* aptamer for lysine. To account for this, we have used buffer conditions that closely approximate those of the kinetic and thermodynamic binding studies [70 mM Tris–HCl (pH 8.0), 20 mM NaCl, 10 mM KCl, and 5 mM Mg^{2+}] with the exception of lower NaCl concentrations (20 mM *versus* 100 mM) that have no influence on the observed binding affinity for lysine (data not shown).

Transcription assays performed at low NTP concentrations (50 μM) revealed an apparent T_{50} of 61 ± 9 μM for lysine, approximately equal to the $K_{d,app}$ (53 ± 5 μM) when the quantified data are fit to a two-state transition model (Fig. 7a and b and Table 3). This observation is consistent with kinetic simulations

Table 3. Comparison of K_d and regulatory efficiency at different transcription speeds

Ligand	K_d (μM)	$T_{50\text{-}50\ \mu M}$ (μM)	$T_{50\text{-}1\ mM}$ (μM)	$K_d/T_{50\text{-}50\ \mu M}$	$K_d/T_{50\text{-}1\ mM}$	ΔT_{50} (1 mM/50 μM NTPs)
Lysine	53 ± 6	61 ± 9	290 ± 50	0.87	0.18	4.8
Lys(−KCl)	480 ± 40	525 ± 50	5500 ± 1400	0.91	0.09	10.5
LysN	90 ± 30	500 ± 200	250 ± 150	0.18	0.36	0.5
MEL	110 ± 30	670 ± 120	9600 ± 2000	0.16	0.01	14.3
EEL	250 ± 30	540 ± 100	9200 ± 1300	0.46	0.03	17.0
KG	570 ± 70	720 ± 460	920 ± 180	0.79	0.62	1.3
6ACA	3100 ± 900	n.d.	n.d.	n.a.	n.a.	n.a.
NML	1670 ± 300	1300 ± 1000	10,000 ± 3800	1.28	0.17	7.7
IEL	1100 ± 290	840 ± 120	n.d.	1.31	n.a.	n.a.
ACL	1700 ± 100	1500 ± 200	n.d.	1.13	n.a.	n.a.
FL	5600 ± 1700	2300 ± 700	n.d.	2.43	n.a.	n.a.

n.d., not detectable.
n.a., not applicable.

above predicting the riboswitch to be under thermodynamic control under slow transcription speeds. These data also argue that previous reports indicating a 1000-fold difference between the K_d (~1 μM) and T_{50} (~1 mM)[23,25,39] can be largely attributed to the differences in the experimental conditions used for binding and transcription studies rather than to binding kinetics. The close agreement between the $K_{d,app}$ and $T_{50,app}$ also suggests that folding of the aptamer into a binding-competent state occurs on a timescale that does not significantly influence the binding reaction. In support of this hypothesis, polymer models of RNA folding would predict a folding time constant of 0.175 s based on the 170-nt chain length of the lysine aptamer domain.[60]

One issue with the above experiment is that the concentration of NTPs used (50 μM) is much less than that found within rapidly growing *E. coli*.[43] Instead, this condition corresponds to the lower limit of the NTP concentrations found in stationary-phase cells.[23,33,61,62] To further define the relationship between binding kinetics and regulatory response, we measured the T_{50} for lysine over a range of NTP concentrations, which increases the rate of nucleotide incorporation and thereby decreases Δt_{RNAP} (Fig. 7c). Between 50 and 400 μM NTPs, we observed no significant change in the T_{50}; however, a relatively sharp increase is observed at concentrations between 400 and 800 μM, reaching a maximum of ~290 μM for lysine at high NTP concentrations (Table 3). This ~5-fold change in the regulatory response agrees extremely well with our kinetic data at the expected extremes for transcription speed (Fig. 6c and d). We also observed that the dynamic range of the regulatory response decreases slightly as a function of transcription speed (Fig. 7d), suggesting that, at rapid transcription speeds, the terminator element has insufficient time to form before the RNAP escapes the uridine-rich tract. Similar loss of regulatory efficiency has been observed for transcriptional regulation of the *trp* operon by the RNA binding TRAP protein.[63]

To assess the effects of altered ligand contacts on the specificity of the regulatory response, we tested various lysine analogs for their ability to regulate transcription using NTP concentrations of 50 μM and 1 mM, respectively (Fig. 8). Under slow transcription conditions, the regulatory response closely approximates the $K_{d,obs}$ for most analogs ($T_{50\text{-}50\ \mu M}$; orange bars), again consistent with kinetic predictions. In contrast, the regulatory behaviors for many of the analogs deviate from kinetic expectations at high NTP concentrations ($T_{50\text{-}1\ mM}$; red bars). For example, the carboxyl ester analogs MEL and EEL are required at significantly higher concentrations than can be accounted for by their binding kinetics (Table 2). Likewise, perturbation of the side-chain contacts has significant influence

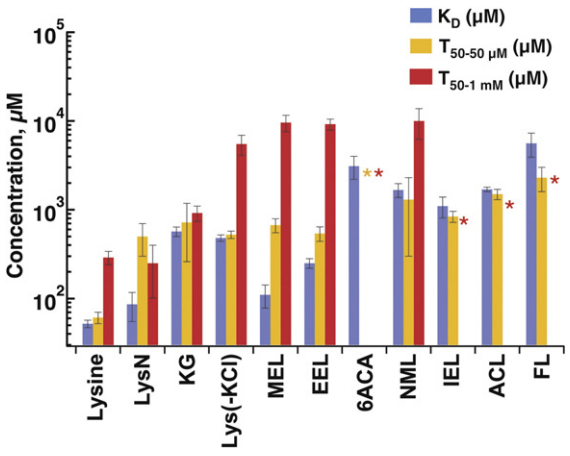

Fig. 8. Comparison of the T_{50} measurements for the various lysine analogs to their $K_{d,app}$ measurements (blue bars) as determined by fluorescence spectroscopy by the 2AP-labeled construct. The observed T_{50} at "slow" (50 μM NTPs; orange bars) and "fast" (1 mM NTPs; red bars) transcription conditions reveal that most lysine analogs are sensitive to the rate of transcription. The absence of T_{50} bars for some compounds indicates that these ligands were unable to elicit regulation under the conditions indicated. The *y*-axis is on a log scale.

on the regulatory response of the RNA at high NTP concentrations. While the regulatory behavior of NML is consistent with the kinetic predictions, side-chain analogs that delocalize or neutralize this charge are unable to regulate at any of the concentrations tested (up to 50 mM) (Fig. 8 and Table 3). Surprisingly, loss of the main-chain amine had the most pronounced effect on regulation, as 6ACA exhibited no apparent activity at any of the transcription conditions tested. Collectively, these data imply that proper placement of the positively charged amines provides added selectivity for lysine during rapid transcription, while the carboxylate group helps to anchor the ligand to the P1 element to elicit a regulatory response. These data further indicate that the slower association rates observed for many non-cognate ligands may hinder their regulatory activities, while increased binding rates impart an efficient regulatory response regardless of transcription speed.

Discussion

Lysine biosynthesis is an important aspect of normal cellular metabolism beyond its requirement as a component of proteins. Key intermediates of lysine biosynthesis such as *meso*-diaminopimelate and dihydropicolinate are essential for cell wall viability and sporulation in bacteria, and thus, numerous mechanisms for controlling this important metabolic pathway have evolved.[24,64] In this study, we have further explored how lysine riboswitch achieves selectivity using a series of chemical analogs that present specific challenges to recognition of polar functional groups of lysine. Previous studies of this riboswitch have hypothesized that its specificity for L-lysine over related cellular metabolites is primarily mediated by appropriate placement of the charged ε-amine.[25,39] Our data demonstrate that, while placement of the ε-amine is required to productively interact with the RNA, a formal charge is not essential. This reflects the highly favorable hydrogen bonding network formed with the ε-amine both by solvent-mediated contacts and by direct interactions with the backbone of the RNA.

Additional binding selectivity for lysine is gained by forming relatively weak interactions with main-chain atoms, thereby prohibiting more promiscuous amino acid binding, certainly a reflection of this selective pressure on the aptamer domain in its biological context. Previous studies focused primarily upon the methylene groups of the side chain and showed that the aptamer can accommodate even relatively bulky groups such as a sulfonyl group at the C4 position.[39] Combined with our data on the tolerance of the RNA to bulky modifications of the carboxylate group, it is clear that this RNA can bind a variety of nonnatural lysine analogs with relatively high affinity, perhaps reflecting the excess volume of the binding cavity (188 $Å^3$) compared with that of lysine (116 $Å^3$). In contrast, other riboswitch classes such as the purine riboswitch form tightly enclosed binding sites that preclude the presence of additional ligand functionality, resulting in high-affinity interactions only with analogs that have near ideal shape complementarity.[3,65–67] The ability of the lysine riboswitch to productively bind the variety of compounds thus far observed is perhaps most surprising in light of the structural data presented here that argue for nonplasticity of the RNA surrounding the binding site that enforces a strict hydrogen bond donor/acceptor constellation.

While many studies have examined the thermodynamics and kinetics of ligand binding to riboswitch aptamers, this study endeavored to correlate these data with an *in vitro* transcription assay capable of quantifying the regulatory response. To do this, we adopted a kinetic model developed by Wickiser *et al.* and Wickiser [Eq. (1)] that relates the regulatory activity (T_{50}) to kinetic binding parameters (k_{on} and k_{off}) and a time allowed for equilibration as determined by the rate of transcription (Δt_{RNAP}).[50,68] Surprisingly, from this analysis, we observe that, at low NTP concentrations, lysine-dependent regulation is essentially under thermodynamic control in contrast to previous observations.[23,39] However, this is consistent with expectations from calculation of the T50 using experimentally observed binding kinetics and a moderate rate of transcription. This implies that under cellular conditions that slow the rate of transcription such as low NTP concentrations, many riboswitches might be under thermodynamic control. A recent study of the *lysC* riboswitch that utilized the *B. subtilis* polymerase observed moderately lower T_{50} values[69] with respect to our measurements (15 μM for *B. subtilis* RNAP *versus* 53 μM for *E. coli* RNAP). These experiments were performed under comparably low NTP concentration (10 μM *versus* 50 μM in this work) but at significantly higher magnesium concentrations that increase the affinity of the aptamer for lysine (our unpublished data). Nonetheless, comparison of our data with that collected with *B. subtilis* RNAP indicates that the two enzymes are regulated by the *lysC* leader similarly and are under thermodynamic control at low NTP conditions.

At higher NTP concentrations reflecting that found in rapidly dividing cells, regulation dramatically shifts from thermodynamic to kinetic control (Fig. 7b). While these experiments were performed with the *E. coli* RNAP transcribing a *B. subtilis* leader sequence, we expect this observation to be consistent between the two enzymes. *B. subtilis* RNAP is known to be less prone to intrinsic pausing than the *E. coli* enzyme,[36] resulting in faster overall transcription through the leader and thus a shorter Δt_{RNAP}. Since pausing becomes less efficient at

higher NTP concentrations, the T_{50} for *B. subtilis* RNAP could be more easily pushed into a kinetic control regime. However, it is important to note that, in all of these, studies employ minimal transcriptional systems devoid of transcription factors such as NusA and NusG that influence pausing and attenuation.[32,36] Thus, these *in vitro* systems likely fail to capture the true complexity of the factors that influence *in vivo* performance. Nonetheless, the minimal transcription system using *E. coli* RNAP provides new insights regarding the regulatory landscape of riboswitches that requires further investigation in the context of the cell.

It is important to note that our kinetic model does not account for some salient details of the transcriptional response. For example, we observe that 30–40% of the transcripts are terminated in the absence of ligand and a maximal termination efficiency of ~80% under saturating ligand concentrations. This observation is typical of the regulatory response of many riboswitches and reflects aspects of the cotranscriptional folding process that are not ligand dependent and, therefore, excluded from our binding model. A second assumption that we make is a direct relationship between the sequence length and Δt_{RNAP}, which implies that transcription proceeds at a constant rate. This assumption is likely violated as the RNAP elongation complex is prone to transcriptional pausing under many circumstances.[70,71] Transcription pausing not only has the potential to prolong the Δt_{RNAP} for transcription of the expression platform, as demonstrated for the *B. subtilis* FMN riboswitch,[21] but also can play an important role in guiding more efficient folding of large RNAs[72,73] as recently implicated for the B_{12} riboswitch.[74] Differences in the pausing behavior of the RNAP, along with the slow association rates of non-cognate ligands (Table 2), may therefore account for the variable efficacy of lysine analogs to regulate transcription at high NTP concentrations (Fig. 8). The difficulty of identifying pause sites from the primary sequence alone, however, motivates further empirical examination of pausing in the context of this and other riboswitch families.

The influence of NTP concentration on transcription attenuation has been studied for a number of systems including protein-dependent regulation of the *trp* operon,[37,63] tRNA-dependent regulation of the *glyQS* gene,[36] and on the intrinsic efficiency of a variety of rho-independent terminators.[75] As was observed for the *lysC* riboswitch (Fig. 7b), regulation by the cognate effector in these systems is markedly influenced at similar NTP concentrations (400–500 μM) *in vitro*. As transcription attenuation represents a broadly used regulatory mechanism for biosynthetic operons in bacteria,[76] we hypothesize that a collective increase in the sensitivity of attenuation mechanisms provides a global regulatory strategy for optimizing biosynthetic needs under resource-limited conditions. Such a strategy would presumably complement other NTP sensing mechanisms such as those that control pyrimidine biosynthesis[34] and ribosome biosynthesis,[35] the latter being a key determinant of the overall growth rate of bacteria. Further analysis of riboswitch-mediated transcription attenuation will be therefore required to decipher the degree to which different riboswitches couple regulation to global aspects of metabolism and should yield additional insights into how microorganisms tailor their metabolism to function robustly in diverse environmental conditions.

Materials and Methods

Preparation of RNA

A 2AP-modified oligonucleotide with the sequence GGAGUCUUUCUUGGAG-2AP-GCUAUCUCUCC was chemically synthesized by Dharmacon, Inc. All other RNAs in this study were synthesized using T7 RNAP and purified according to previously established protocols.[23,25,39,77] Purified RNAs were stored in 5 mM Tris–HCl (pH 8.0) and 0.5 mM EDTA buffer and stored at −20 °C prior to use.

To assure proper annealing of the two-piece RNA construct, we engineered the sequence derived from the *B. subtilis lysC* aptamer using the following 5′ and 3′ primers to PCR amplify from a cloned plasmid containing the entire promoter and 5′ leader segments of this gene (5′-TAATACGACTACTATAGGCGTGAGCAGACTCTTTTTTGGAGAGATAGAGGTGCGAAC and 3′-TAAACGACCGGCACGTAACTTATTTACATTCCGACAGTTCTTTCTGAGG) to produce an unlabeled RNA with the sequence GGAGAGAUAGAGGUGCGAACUUCAAGAGUAUGCCUUUGGAGAAAGAUGGAUUCUGUGAAAAAGGCUGAAAGGGGAGCGUCGCCGAAGCAAUAAAACCCCAUCGGUAUUAUUUGCUGGCCGUGCAUUGAAUAAAUGUAAGGCUGUCAAGAAAGACUCC.

The two-piece RNA used in the titration experiments was constructed by annealing in a buffer containing 50 mM Na-Hepes (pH 8.0) and 100 mM NaCl. The unlabeled RNA was added to a final concentration of 3 μM to a 1-μM stock of 2AP-labeled RNA and heated in a PCR block to 85 °C for 2 min then cooling at a rate of 0.1 °C/s with a 2-min hold at 10° intervals down to 4 °C. Annealed products were analyzed by native polyacrylamide gel electrophoresis to ensure that the quality of the annealing reaction was optimal. Under these conditions, the labeled oligonucleotide was verified to incorporate with high efficiency into a single species corresponding to the appropriate size product.

Fluorescence spectroscopy

All ligand titrations were carried out in 50 mM Tris–HCl (pH 8.0) and 100 mM NaCl and 5 mM $MgCl_2$ and 10 mM KCl with a 100-nM RNA unless indicated otherwise. Changes in the fluorescence of the 2AP reporter as a function of ligand concentration were measured using a

Tecan 96-well plate reader for all room temperature experiments and in a Chirascan fluorescence spectrometer for 37 °C experiments. Data were fit to the equation

$$\Delta F = F_{min} + (F_{max} - F_{min}) \times \left(\frac{[L]^n}{[L]^n + K_d} \right) \quad (2)$$

where ΔF is the measured change in fluorescence, [L] is the ligand concentration, F_{min} is the initial fluorescence, and $F_{max} - F_{min}$ represents the total magnitude of the change in measured fluorescence change for the titration.

Isothermal titration calorimetry

The wild-type *lysC* riboswitch aptamer from *B. subtilis* (RFAM accession ABQL01000005.1/1891692-1891513) was dialyzed overnight at 4 °C in 50 mM Na-Hepes (pH 8.0), 100 mM NaCl, 5 mM $MgCl_2$, and 10 mM KCl. The RNA was diluted to a final concentration of 60 μM and titrated with lysine that had been dissolved directly in the dialysis buffer at concentrations 10-fold in excess of the RNA. Titrations were all performed at 20 and 37 °C using the VP-ITC microcalorimeter (Microcal, Inc.). Data analysis and fitting was performed with the Origin 5.0 software suite (Origin Laboratories) as previously described.[78]

Chemical probing

Chemical probing was performed essentially as described elsewhere.[79,80] RNA was diluted to 100 nM in 10 μL of a buffer of 50 mM Tris–HCl (pH 8.0), 100 mM NaCl, 50 mM KCl, 5 mM $MgCl_2$, and 0.1 mM EDTA. The RNA was incubated with either 1 mM lysine or 10 mM lysine analog to ensure that binding was at or near saturation. RNA was probed at 37 °C for 45 min with 65 mM NMIA. Reverse transcription was performed by adding 3 μL of ^{32}P-labeled DNA primer (~10 nM final) and heating the solution to 95 °C for 5 min then cooling to 37 °C for 5 min on a PCR block. The solution was then brought to 54 °C before adding 3 μL of a SuperScript III (Life Technologies) reverse transcriptase mix and allowing 10 min for primer extension. The RNA in the reaction was degraded by adding 1 μL of 4 M NaOH and incubating at 95 °C for 5 min before quenching with a 1:1 Tris (unbuffered):formamide solution. Polyacrylamide gel electrophoresis analysis was performed using 12% polyacrylamide gels.

In vitro transcription studies

In vitro transcription assays were performed using the wild-type *lysC* gene from *B. subtilis* containing the T7A1 phage promoter fused at the genomic +1 transcription start site. Template DNA (10 nM) was equilibrated at 37 °C in the presence of 0.5 units of *E. coli* RNAP holoenzyme with saturating α-subunit (Epicentre) in 1× TB1 [70 mM Tris–HCl (pH 8.0), 20 mM NaCl, 5 mM $MgCl_2$, 10 mM KCl, 17 mM DTT, 0.1 mM EDTA, and 35 μg/mL bovine serum albumin] for 10 min prior to the addition of NTP substrate to 50 μM in a final volume of 20 μL. For reactions performed at different NTP concentrations, we adjusted the concentration of Mg^{2+} added to the reaction based on calculations performed with CHELATOR,[81] as implemented by MaxChelator[82] to maintain a constant concentration of free Mg^{2+}.

Following addition of NTPs, the reactions were incubated for 15 min at 37 °C and quenched with an equal volume of 85% formamide. Products were separated by 6% denaturing gel electrophoresis, and counts were obtained by standard phosphorimaging. Total counts for full length and terminated were background corrected and normalized to the total number of A's in each product. Percent termination was plotted and fit to the equation

$$T_{50} = T_{min} + (T_{max} - T_{min}) \times \left(\frac{[L]^n}{[L]^n + K_d} \right) \quad (3)$$

where T_{min} is the observed termination in the absence of ligand and T_{max} is the maximal termination achieved at high ligand concentrations.

Crystallographic data collection and processing

Crystallization of the 6ACA and KG ligands was performed with a variant of the *T. maritima asd* lysine riboswitch that was previously described (PDB ID: 3D0U).[38] The RNA was transcribed, purified, and refolded using previously described protocols[77] and was concentrated to 400 μM in 10 mM Na-Hepes (pH 7.0) and 5 mM $MgCl_2$. RNA and ligand were then mixed at a 10:1 ratio to give a final ligand concentration of 5 mM and allowed to incubate for 30 min prior to setting up crystallization drops. Mother liquor [10 mM Na-Hepes (pH 7.0), 2 M Li_2SO_4, and 5 mM $MgCl_2$] was mixed with the RNA–ligand solution in a 1:1 volumetric ratio, and crystallization was performed by hanging-drop vapor diffusion. Diffraction data were collected on a copper rotating anode source (Rigaku RU200 and Rigaku RU2HR) with a Rigaku MSC IV++ area detector at 100 K. Data were scaled and averaged using the D*TREK[83] as part of the CrystalClear software package (Rigaku MSC). Structures of the 6ACA- and KG-bound complexes were solved by molecular replacement with the unliganded lysine aptamer (PDB ID: 3D0X) using the PHENIX software suite.[84] Model building was performed with Coot,[85] and additional refinement was performed with the routines implemented in PHENIX. All figures of structural models were prepared using PyMOL.[86]

Accession numbers

Coordinates and structure factors have been deposited in the PDB under the accession numbers 4ERJ (6ACA bound) and 4ERL (KG bound).

Acknowledgements

The authors would like to thank Benedict Ifedi for his assistance in the initial development of the two-piece lysine reporter RNA as part of the Summer Multicultural Access to Research Training program

at the University of Colorado at Boulder. This work was supported by grants from the National Institutes of Health (R01 GM073850 and 1S10 RR026516) to R.T.B. and an NIH/CU Molecular Biophysics Training Program (T32 GM065103) to A.D.G.

Supplementary Data

Supplementary data to this article can be found online at http://dx.doi.org/10.1016/j.jmb.2012.06.038

References

1. Breaker, R. R. (2012). Riboswitches and the RNA world. *Cold Spring Harb. Perspect. Biol*. Feb 1;**4**. pii: a003566. http://dx.doi.org/10.1101/cshperspect.a003566.
2. Montange, R. K. & Batey, R. T. (2008). Riboswitches: emerging themes in RNA structure and function. *Annu. Rev. Biophys.* **37**, 117–133.
3. Mandal, M., Boese, B., Barrick, J. E., Winkler, W. C. & Breaker, R. R. (2003). Riboswitches control fundamental biochemical pathways in *Bacillus subtilis* and other bacteria. *Cell*, **113**, 577–586.
4. Batey, R. T., Gilbert, S. D. & Montange, R. K. (2004). Structure of a natural guanine-responsive riboswitch complexed with the metabolite hypoxanthine. *Nature*, **432**, 411–415.
5. Serganov, A., Yuan, Y.-R., Pikovskaya, O., Polonskaia, A., Malinina, L., Phan, A. T. *et al.* (2004). Structural basis for discriminative regulation of gene expression by adenine- and guanine-sensing mRNAs. *Chem. Biol.* **11**, 1729–1741.
6. Winkler, W. C., Nahvi, A., Roth, A., Collins, J. A. & Breaker, R. R. (2004). Control of gene expression by a natural metabolite-responsive ribozyme. *Nature*, **428**, 281–286.
7. Ames, T. D., Rodionov, D. A., Weinberg, Z. & Breaker, R. R. (2010). A eubacterial riboswitch class that senses the coenzyme tetrahydrofolate. *Chem. Biol.* **17**, 681–685.
8. Nahvi, A., Sudarsan, N., Ebert, M. S., Zou, X., Brown, K. L. & Breaker, R. R. (2002). Genetic control by a metabolite binding mRNA. *Chem. Biol.* **9**, 1043.
9. Sudarsan, N., Lee, E. R., Weinberg, Z., Moy, R. H., Kim, J. N., Link, K. H. & Breaker, R. R. (2008). Riboswitches in eubacteria sense the second messenger cyclic di-GMP. *Science*, **321**, 411–413.
10. Montange, R. K., Mondragón, E., Van Tyne, D., Garst, A. D., Ceres, P. & Batey, R. T. (2010). Discrimination between closely related cellular metabolites by the SAM-I riboswitch. *J. Mol. Biol.* **396**, 761–772.
11. Gilbert, S. D., Rambo, R. P., Van Tyne, D. & Batey, R. T. (2008). Structure of the SAM-II riboswitch bound to *S*-adenosylmethionine. *Nat. Struct. Mol. Biol.* **15**, 177–182.
12. Batey, R. T. (2011). Recognition of *S*-adenosylmethionine by riboswitches. *Wiley Interdiscip. Rev.: RNA*, **2**, 299–311.
13. Lu, C., Smith, A. M., Fuchs, R. T., Ding, F., Rajashankar, K., Henkin, T. M. & Ke, A. (2008). Crystal structures of the SAM-III/S_{MK} riboswitch reveal the SAM-dependent translation inhibition mechanism. *Nat. Struct. Mol. Biol.* **15**, 1076–1083.
14. Thore, S., Leibundgut, M. & Ban, N. (2006). Structure of the eukaryotic thiamine pyrophosphate riboswitch with its regulatory ligand. *Science*, **312**, 1208–1211.
15. Serganov, A., Polonskaia, A., Phan, A. T., Breaker, R. R. & Patel, D. J. (2006). Structural basis for gene regulation by a thiamine pyrophosphate-sensing riboswitch. *Nature*, **441**, 1167–1171.
16. Serganov, A., Huang, L. & Patel, D. J. (2009). Coenzyme recognition and gene regulation by a flavin mononucleotide riboswitch. *Nature*, **458**, 233–237.
17. Serganov, A., Huang, L. & Patel, D. J. (2008). Structural insights into amino acid binding and gene control by a lysine riboswitch. *Nature*, **455**, 1263–1267.
18. Blount, K. F. & Breaker, R. R. (2006). Riboswitches as antibacterial drug targets. *Nat. Biotechnol.* **24**, 1558–1564.
19. Barrick, J. E. & Breaker, R. R. (2007). The distributions, mechanisms, and structures of metabolite-binding riboswitches. *Genome Biol.* **8**, R239.
20. Link, K. H. & Breaker, R. R. (2009). Engineering ligand-responsive gene-control elements: lessons learned from natural riboswitches. *Gene Ther.* **16**, 1189–1201.
21. Wickiser, J. K., Winkler, W. C., Breaker, R. R. & Crothers, D. M. (2005). The speed of RNA transcription and metabolite binding kinetics operate an FMN riboswitch. *Mol. Cell*, **18**, 49–60.
22. Lemay, J.-F., Desnoyers, G., Blouin, S., Heppell, B., Bastet, L., St-Pierre, P. *et al.* (2011). Comparative study between transcriptionally- and translationally-acting adenine riboswitches reveals key differences in riboswitch regulatory mechanisms. *PLoS Genet.* **7**, e1001278.
23. Blouin, S. & Lafontaine, D. A. (2007). A loop loop interaction and a K-turn motif located in the lysine aptamer domain are important for the riboswitch gene regulation control. *RNA*, **13**, 1256–1267.
24. Grundy, F. J., Lehman, S. C. & Henkin, T. M. (2003). The L box regulon: lysine sensing by leader RNAs of bacterial lysine biosynthesis genes. *Proc. Natl Acad. Sci. USA*, **100**, 12057–12062.
25. Sudarsan, N., Wickiser, J. K., Nakamura, S., Ebert, M. S. & Breaker, R. R. (2003). An mRNA structure in bacteria that controls gene expression by binding lysine. *Genes Dev.* **17**, 2688–2697.
26. Tomsic, J., McDaniel, B. A., Grundy, F. J. & Henkin, T. M. (2008). Natural variability in *S*-adenosylmethionine (SAM)-dependent riboswitches: S-box elements in *Bacillus subtilis* exhibit differential sensitivity to SAM *In vivo* and *in vitro*. *J. Bacteriol.* **190**, 823–833.
27. Smith, K. D., Lipchock, S. V., Livingston, A. L., Shanahan, C. A. & Strobel, S. A. (2010). Structural and biochemical determinants of ligand binding by the c-di-GMP riboswitch. *Biochemistry*, **49**, 7351–7359.
28. Trausch, J. J., Ceres, P., Reyes, F. E. & Batey, R. T. (2011). The structure of a tetrahydrofolate-sensing riboswitch reveals two ligand binding sites in a single aptamer. *Structure*, **19**, 1413–1423.
29. Artsimovitch, I. & Landick, R. C. (2000). Pausing by bacterial RNA polymerase is mediated by mechanistically distinct classes of signals. *Proc. Natl Acad. Sci. USA*, **97**, 7090–7095.

30. Ha, K. S., Toulokhonov, I., Vassylyev, D. G. & Landick, R. C. (2010). The NusA N-terminal domain is necessary and sufficient for enhancement of transcriptional pausing via interaction with the RNA exit channel of RNA polymerase. *J. Mol. Biol.* **401**, 708–725.
31. Yakhnin, A. V., Yakhnin, H. & Babitzke, P. (2008). Function of the *Bacillus subtilis* transcription elongation factor NusG in hairpin-dependent RNA polymerase pausing in the *trp* leader. *Proc. Natl Acad. Sci. USA*, **105**, 16131–16136.
32. Yakhnin, A. V. & Babitzke, P. (2002). NusA-stimulated RNA polymerase pausing and termination participates in the *Bacillus subtilis trp* operon attenuation mechanism *in vitro*. *Proc. Natl Acad. Sci. USA*, **99**, 11067–11072.
33. Buckstein, M. H., He, J. & Rubin, H. (2008). Characterization of nucleotide pools as a function of physiological state in *Escherichia coli*. *J. Bacteriol.* **190**, 718–726.
34. Turnbough, C. L. & Switzer, R. L. (2008). Regulation of pyrimidine biosynthetic gene expression in bacteria: repression without repressors. *Microbiol. Mol. Biol. Rev.* **72**, 266–300.
35. Gaal, T., Bartlett, M. S., Ross, W., Turnbough, C. L. & Gourse, R. L. (1997). Transcription regulation by initiating NTP concentration: rRNA synthesis in bacteria. *Science*, **278**, 2092–2097.
36. Grundy, F. J. & Henkin, T. M. (2004). Kinetic analysis of tRNA-directed transcription antitermination of the *Bacillus subtilis glyQS* gene *in vitro*. *J. Bacteriol.* **186**, 5392–5399.
37. McGraw, A. P., Bevilacqua, P. C. & Babitzke, P. (2007). TRAP-5′ stem–loop interaction increases the efficiency of transcription termination in the *Bacillus subtilis trpEDCFBA* operon leader region. *RNA*, **13**, 2020–2033.
38. Garst, A. D., Heroux, A., Rambo, R. P. & Batey, R. T. (2008). Crystal structure of the lysine riboswitch regulatory mRNA element. *J. Biol. Chem.* **283**, 22347–22351.
39. Blount, K. F., Wang, J. X., Lim, J., Sudarsan, N. & Breaker, R. R. (2007). Antibacterial lysine analogs that target lysine riboswitches. *Nat. Chem. Biol.* **3**, 44–49.
40. Baird, N. J., Gong, H., Zaheer, S. S., Freed, K. F., Pan, T. & Sosnick, T. R. (2010). Extended structures in RNA folding intermediates are due to nonnative interactions rather than electrostatic repulsion. *J. Mol. Biol.* **397**, 1298–1306.
41. Baird, N. J. & Ferré-D'Amaré, A. R. (2010). Idiosyncratically tuned switching behavior of riboswitch aptamer domains revealed by comparative small-angle X-ray scattering analysis. *RNA*, **16**, 598–609.
42. Watson, P. Y. & Fedor, M. J. (2011). The glmS riboswitch integrates signals from activating and inhibitory metabolites *in vivo*. *Nat. Struct. Mol. Biol.* **18**, 359–363.
43. Bennett, B. D., Kimball, E. H., Gao, M., Osterhout, R., Van Dien, S. J. & Rabinowitz, J. D. (2009). Absolute metabolite concentrations and implied enzyme active site occupancy in *Escherichia coli*. *Nat. Methods*, **5**, 593–599.
44. Merino, E. J., Wilkinson, K. A., Coughlan, J. L. & Weeks, K. M. (2005). RNA structure analysis at single nucleotide resolution by selective 2′-hydroxyl acylation and primer extension (SHAPE). *J. Am. Chem. Soc.* **127**, 4223–4231.
45. McGinnis, J. L., Dunkle, J. A., Cate, J. H. D. & Weeks, K. M. (2012). The mechanisms of RNA SHAPE chemistry. *J. Am. Chem. Soc.* **134**, 6617–6624.
46. Gherghe, C. M., Shajani, Z., Wilkinson, K. A., Varani, G. & Weeks, K. M. (2008). Strong correlation between SHAPE chemistry and the generalized NMR order parameter (S2) in RNA. *J. Am. Chem. Soc.* **130**, 12244–12245.
47. Theobald, D. L. & Wuttke, D. S. (2006). THESEUS: maximum likelihood superpositioning and analysis of macromolecular structures. *Bioinformatics*, **22**, 2171–2172.
48. Breaker, R. R. (2011). Prospects for riboswitch discovery and analysis. *Mol. Cell*, **43**, 867–879.
49. Goodrich, J. A. & Kugel, J. F. (2007). *Binding and Kinetics for Molecular Biologists*. Cold Spring Harbor Laboratory Press, Cold Spring Harbor, NY.
50. Wickiser, J. K., Cheah, M. T., Breaker, R. R. & Crothers, D. M. (2005). The kinetics of ligand binding by an adenine-sensing riboswitch. *Biochemistry*, **44**, 13404–13414.
51. Korzheva, N., Mustaev, A., Kozlov, M., Malhotra, A., Nikiforov, V., Goldfarb, A. & Darst, S. A. (2000). A structural model of transcription elongation. *Science*, **289**, 619–625.
52. Proshkin, S., Rahmouni, A. R., Mironov, A. & Nudler, E. (2010). Cooperation between translating ribosomes and RNA polymerase in transcription elongation. *Science*, **328**, 504–508.
53. Vogel, U. & Jensen, K. F. (1994). The RNA chain elongation rate in *Escherichia coli* depends on the growth rate. *J. Bacteriol.* **176**, 2807–2813.
54. Zhou, J., Ha, K. S., La Porta, A., Landick, R. C. & Block, S. M. (2011). Applied force provides insight into transcriptional pausing and its modulation by transcription factor NusA. *Mol. Cell*, **44**, 635–646.
55. Taniguchi, Y., Choi, P. J., Li, G.-W., Chen, H., Babu, M., Hearn, J. *et al.* (2010). Quantifying *E. coli* proteome and transcriptome with single-molecule sensitivity in single cells. *Science*, **329**, 533–538.
56. Artsimovitch, I. & Henkin, T. M. (2009). *In vitro* approaches to analysis of transcription termination. *Methods*, **47**, 37–43.
57. Landick, R. C., Wang, D. & Chan, C. L. (1996). Quantitative analysis of transcriptional pausing by *Escherichia coli* RNA polymerase: his leader pause site as paradigm. *Methods Enzymol.* **274**, 334–353.
58. Artsimovitch, I., Svetlov, V., Anthony, L., Burgess, R. R. & Landick, R. C. (2000). RNA polymerases from *Bacillus subtilis* and *Escherichia coli* differ in recognition of regulatory signals *in vitro*. *J. Bacteriol.* **182**, 6027–6035.
59. Ray, P. S., Jia, J., Yao, P., Majumder, M., Hatzoglou, M. & Fox, P. L. (2009). A stress-responsive RNA switch regulates VEGFA expression. *Nature*, **457**, 915–919.
60. Hyeon, C. & Thirumalai, D. (2012). Chain length determines the folding rates of RNA. *Biophys. J.* **102**, L11–L13.
61. Ryals, J., Little, R. & Bremer, H. (1982). Temperature dependence of RNA synthesis parameters in *Escherichia coli*. *J. Bacteriol.* **151**, 879–887.

62. Poulsen, P. & Jensen, K. F. (1987). Effect of UTP and GTP pools on attenuation at the *pyrE* gene of *Escherichia coli*. *Mol. Gen. Genet.* **208**, 152–158.
63. Barbolina, M. V., Kristoforov, R., Manfredo, A., Chen, Y. & Gollnick, P. (2007). The rate of TRAP binding to RNA is crucial for transcription attenuation control of the *B. subtilis trp* operon. *J. Mol. Biol.* **370**, 925–938.
64. Rodionov, D. A., Vitreschak, A. G., Mironov, A. A. & Gelfand, M. S. (2003). Regulation of lysine biosynthesis and transport genes in bacteria: yet another RNA riboswitch? *Nucleic Acids Res.* **31**, 6748–6757.
65. Gilbert, S. D., Mediatore, S. J. & Batey, R. T. (2006). Modified pyrimidines specifically bind the purine riboswitch. *J. Am. Chem. Soc.* **128**, 14214–14215.
66. Gilbert, S. D., Reyes, F. E., Edwards, A. L. & Batey, R. T. (2009). Adaptive ligand binding by the purine riboswitch in the recognition of guanine and adenine analogs. *Structure*, **17**, 857–868.
67. Daldrop, P., Reyes, F. E., Robinson, D. A., Hammond, C. M., Lilley, D. M., Batey, R. T. & Brenk, R. (2011). Novel ligands for a purine riboswitch discovered by RNA–ligand docking. *Chem. Biol.* **18**, 324–335.
68. Wickiser, J. K. (2009). Kinetics of riboswitch regulation studied by *in vitro* transcription. *Methods Mol. Biol.* **540**, 53–63.
69. Wilson-Mitchell, S. N., Grundy, F. J. & Henkin, T. M. (2012). Analysis of lysine recognition and specificity of the *Bacillus subtilis* L box riboswitch. *Nucleic Acids Res.* **40**, 5706–5717.
70. Uptain, S. M., Kane, C. M. & Chamberlin, M. J. (1997). Basic mechanisms of transcript elongation and its regulation. *Annu. Rev. Biochem.* **66**, 117–172.
71. Herbert, K. M., La Porta, A., Wong, B. J., Mooney, R. A., Neuman, K. C., Landick, R. C. & Block, S. M. (2006). Sequence-resolved detection of pausing by single RNA polymerase molecules. *Cell*, **125**, 1083–1094.
72. Pan, T., Artsimovitch, I., Fang, X. W., Landick, R. C. & Sosnick, T. R. (1999). Folding of a large ribozyme during transcription and the effect of the elongation factor NusA. *Proc. Natl Acad. Sci. USA*, **96**, 9545–9550.
73. Wong, T. N., Sosnick, T. R. & Pan, T. (2007). Folding of noncoding RNAs during transcription facilitated by pausing-induced nonnative structures. *Proc. Natl Acad. Sci. USA*, **104**, 17995–18000.
74. Perdrizet, G. A., Artsimovitch, I., Furman, R., Sosnick, T. R. & Pan, T. (2012). Transcriptional pausing coordinates folding of the aptamer domain and the expression platform of a riboswitch. *Proc. Natl Acad. Sci. USA*, **109**, 3323–3328.
75. McDowell, J. C., Roberts, J. W., Jin, D. J. & Gross, C. A. (1994). Determination of intrinsic transcription termination efficiency by RNA polymerase elongation rate. *Science*, **266**, 822–825.
76. Merino, E. & Yanofsky, C. (2005). Transcription attenuation: a highly conserved regulatory strategy used by bacteria. *Trends Genet.* **21**, 260–264.
77. Edwards, A. L., Garst, A. D. & Batey, R. T. (2009). Determining structures of RNA aptamers and riboswitches by X-ray crystallography. *Methods Mol. Biol.* **535**, 135–163.
78. Gilbert, S. D., Stoddard, C. D., Wise, S. J. & Batey, R. T. (2006). Thermodynamic and kinetic characterization of ligand binding to the purine riboswitch aptamer domain. *J. Mol. Biol.* **359**, 754–768.
79. Steen, K.-A., Siegfried, N. A. & Weeks, K. M. (2011). Selective 2′-hydroxyl acylation analyzed by protection from exoribonuclease (RNase-detected SHAPE) for direct analysis of covalent adducts and of nucleotide flexibility in RNA. *Nat. Protoc.* **6**, 1683–1694.
80. Stoddard, C. D., Gilbert, S. D. & Batey, R. T. (2008). Ligand-dependent folding of the three-way junction in the purine riboswitch. *RNA*, **14**, 675–684.
81. Schoenmakers, T. J., Visser, G. J., Flik, G. & Theuvenet, A. P. (1992). CHELATOR: an improved method for computing metal ion concentrations in physiological solutions.*BioTechniques*, **12**; 870–4-876–9.
82. Bers, D. M., Patton, C. W. & Nuccitelli, R. (1994). A practical guide to the preparation of Ca^{2+} buffers. *Methods Cell Biol.* **40**, 3–29.
83. Pflugrath, J. W. (1999). The finer things in X-ray diffraction data collection. *Acta Crystallogr., Sect. D: Biol. Crystallogr.* **55**, 1718–1725.
84. Adams, P. D., Afonine, P. V., Bunkóczi, G., Chen, V. B., Davis, I. W., Echols, N. *et al.* (2010). PHENIX: a comprehensive Python-based system for macromolecular structure solution. *Acta Crystallogr., Sect. D: Biol. Crystallogr.* **66**, 213–221.
85. Emsley, P. & Cowtan, K. (2004). Coot: model-building tools for molecular graphics. *Acta Crystallogr., Sect. D: Biol. Crystallogr.* **60**, 2126–2132.
86. DeLano, W. (2002). The PyMOL Molecular Graphics System DeLano Scientific, San Carlos, CA.